Mechanical and Servo System Performance of the ESA Deep Space Antennas

Konrad Pausch [1], Markus Omlor[1], Uwe Mutzberg [1], Peter Droll [2]

[1] ***Vertex Antennentechnik***
Baumstr. 50, D-47198 Duisburg, Germany
Email: kpausch@vertexant.de

[2] ***European Space Operations Centre***
Robert-Bosch-Strasse 5, D-64293 Darmstadt, Germany
Email: peter.droll@esa.int

INTRODUCTION

ESOC has build two deep space antennas in New Norcia/ Australia (DSA1) and Cebreros/ Spain (DSA2) to support ESA's interplanetary missions. A third antenna is planned for 2010. The design of the antenna system is the result of the demanding requirements in terms of performance originated from the Rosetta mission, but taking into account also planned future missions like Bepi Colombo. The derived requirements with respect to the pointing and surface accuracy have been the key design drivers for the mechanical structure of the antennas. In view of the required support to future Ka-Band missions, only pointing errors of a few millidegrees can be tolerated. Already 5.5 mdeg pointing error result in 1.2 dB pointing loss. Due to the challenging system availability requirements, the performance of the system has to be ensured under worst case wind and temperature conditions.

Figure 1: ESA's 35 m antenna at Cebreros (Spain).

SYSTEM REQUIREMENTS

The two deep space ground stations have a common system architecture and employ similar or identical components at the level of mechanical, servo, RF, IF and baseband subsystems [1]. The required G/T and EIRP triggered the selection of the antenna diameter of 35m. The hereby assumed reflector surface and pointing requirements were the starting point for the design of the antenna mechanics and the servo system.

In Table 1, the mechanical and servo requirements are summarized. The defined surface accuracy and pointing accuracy values have to be achieved within the full azimuth and elevation travel range under up to 45 km/h constant wind with wind gusts up to 60 km/h.

Table 1: Mechanical and Servo Requirements.

Requirement	Value
Azimuth travel range	0^o to 480^o (DSA1) and 0^o to 540^o (DSA2)
Elevation travel range	0^o to 90^o
Maximum slew rate, either axis	$\geq$ 0.4 deg/s (DSA1) and $\geq$ 1.0 deg/s (DSA2)
Maximum acceleration, either axis	$\geq$ 0.4 deg/s^2 (DSA1) and $\geq$ 1.0 deg/s^2 (DSA2)
Pointing error (99 % probability of occurrence)	S-band: $\leq$ 26 mdeg X-band: $\leq$ 11 mdeg (DSA1) and $\leq$ 5.5 mdeg (DSA2) Ka-band: $\leq$ 5.5 mdeg
Main reflector surface accuracy	$\leq$ 0.3 mm r.m.s.
Subreflector surface accuracy	$\leq$ 0.12 mm r.m.s.
Operational wind	45 km/h constant gusting to 60 km/h.
Operational temperature	-20 ^{o}C to 50 ^{o}C

MECHANICAL AND SERVO SYSTEM DESIGN

The requirements with respect to the pointing and surface accuracy are the key design drivers for the mechanical structure of the antennas. In a design study, which preceded the contract for the DSA1, different mechanical design concepts were studied and compared with respect to the achievable performance. The chosen design is a full motion turning head pedestal with a Beam Wave Guide (BWG) concept (Fig. 1). The mechanical part of the antenna system comprises an elevation structure (main- and subreflector, ballast cantilever) supported by the azimuth housing, which is mounted on top of the antenna tower. The tower also serves as the antenna equipment room (AER), hosting the feeds and electronic equipment. The turning head design also allows BWG mirrors, drive motors and gearboxes to be located within the antenna structure to provide environmental protection and convenient access for maintenance.

The rotating azimuth portion is a three story steel structure that supports the elevation axis on two fixed bearings (Fig. 2). It houses the elevation and azimuth drives and encoders as well as the moveable elements of the BWG. The azimuth motion is accomplished by two gearboxes each fitted with two servo motors. The elevation motion is realized by four gearboxes with one servo motor each, engaging toothed gear segments on the two ballast cantilevers. The azimuth housing is mounted on the antenna tower by means of an extremely stiff three-row-roller bearing and a fixed steel base ring with an integral azimuth ring gear. Apart from horizontal and vertical loads, this bearing also transmits tilting moments, resulting from wind and seismic loads, to the tower/foundation.

The main and subreflector supporting structure and the azimuth housing, which are made out of steel, are not isolated. To reduce nevertheless the impact of ambient temperature changes, the mechanical structure is symmetrical to the maximum extent.

A detailed Finite-Element model of the antenna was used to determine the mechanical deformations for different load cases including gravity, thermal and wind effects for various elevation angles. The FE models consist of approximately 18 700 elements with ca. 17 100 nodal points and 100 000 local degrees of freedom (Fig. 3).

In order to obtain a mechanical design with optimal performance with respect to pointing accuracy and surface accuracy, the structure was subject to mathematical optimization. A sequential optimization of a multi-objective quadratic problem according to a modified JACOB approach has been used. This algorithm allows fast simultaneous

optimization of different parameters of large structural Finite-Element models. The reflector truss topology, backup structure cross sections and azimuth house wall thicknesses have been optimized for mass, surface r.m.s. and pointing performance under wind and gravitational loads. Furthermore the main azimuth house wall thicknesses were designed after mathematical optimization with respect to pointing error contributions of the azimuth house. The optimization process was a basic prerequisite to achieve the specified mechanical performance. It has been stopped when the predicted performance showed compliance with the specification.

As a result, the reflector supporting structure consists of the existing truss topology (Fig. 2) in which each truss type has an individual outer diameter and wall thickness. The supporting structure has a weight of 90 tons, which is only 25 % of the total weight of the moving elevation part. The ballast cantilevers (box structures made out of steel and filled with concrete) used to counterbalance the reflector weight of 240 tons.

Figure 2: Concrete tower, azimuth and elevation portion of the antenna.

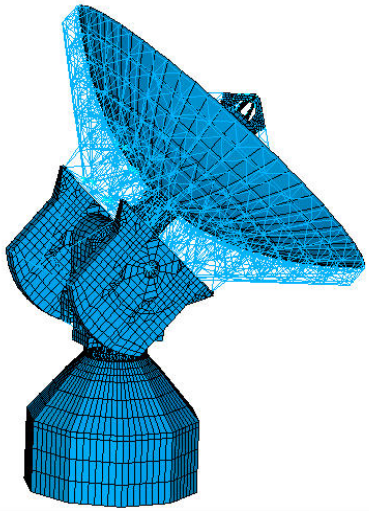

Figure 3: Topology of the Finite Element Model at 50° elevation position.

In particular the servo system is a dominant source of non-systematic pointing errors. In order to optimize the servo control loops and to predict the final antenna servo performance, the antenna was analysed with dynamical simulations. The used simulation models were derived from the Finite Element model of the entire antenna. As models of this size are not suitable for dynamic simulations, the model size was reduced by modal analysis technique. This led to reduced order mechanical simulation models, which consist of 28 coupled differential equations of 2nd order. These models take into account all resonance modes and hereby all dynamic antenna characteristics in the critical frequency range up to 10 Hz. Nonlinear mechanical effects as gearbox backlash, gearbox and bearing friction were also taken into account. Finally the antenna simulation model was completed by models of the digital controllers with encoders and tachos and by the servo amplifiers. Pointing error components due to the servo wind gust rejection are minimized by highly optimized servo controllers. The final controller design and the corresponding controller parameters were validated by dynamical simulations of various operation modes as well as by sensitivity analyses. The theoretically derived controller parameters were implemented into the ACU with only very minor adaptations on site. This approach led to very good accordance between the dynamical behaviour of the theoretically developed antenna simulation model, which includes nonlinearities as limitation-, quantization- and cycling time effects and the behaviour of the real antenna. Fig. 4 exemplarily shows the azimuth and elevation position error due to 50 km/h side-wind respectively front-wind with gusts up to 70 km/h at 45 deg elevation. For these cases the azimuth position error is less than 0.3 mdeg and the elevation position error is less than 0.2 mdeg (r.m.s).

To meet the specified pointing requirements, the design of the mechanical part and of the antenna servo system was systematically analyzed and optimized with respect to their contribution to the overall pointing error budget. The contributions, which result in a non-systematic error (backlash, encoder mounting, servo loop limit cycle, etc.), were minimized by e.g. load dependent backlash compensation, on-site calibration of the off-axis mounted azimuth encoder and minimizing the overall friction.

It is obvious, that also the high stiffness of the elevation part contributes to the very low overall non-systematic pointing error contribution, which is less than 2 mdeg (99 % probability of occurrence) under worst case conditions including wind. The systematic pointing errors introduced by gravity, misalignment, beam squint due to the BWG/feed arrangement, quasi static thermal effects and quasi-constant wind have been minimized by design measures as far as technically and economically feasible. Due to design measures, the sum of the raw and uncompensated systematic errors is dominated by the gravity effects and has a value of approximately 100 mdeg (Table 2). The compensation of these pointing errors is crucial for achieving the specified pointing accuracy.

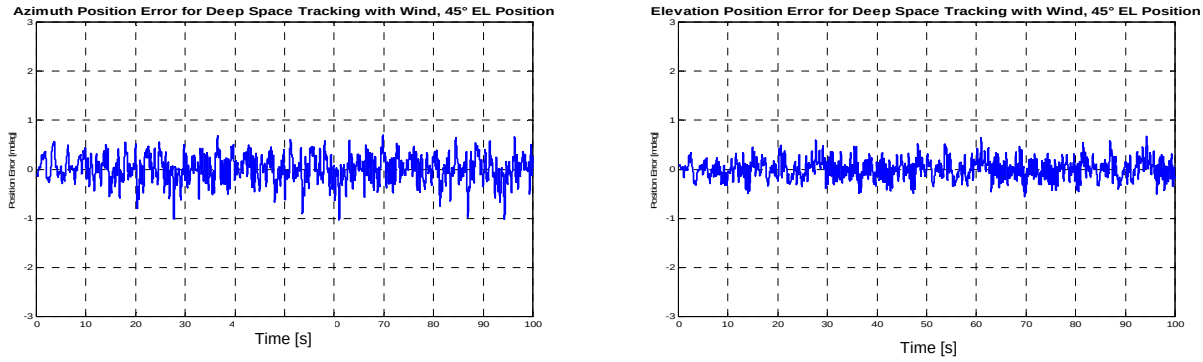

Figure 4: Simulated azimuth and elevation position error in [mdeg]. Load case: 50 km/h side-wind with gusts up to 70 km/h.

Therefore the servo system is able to compensate pointing errors introduced by gravity deformation, mechanical misalignments, beam-squint due to the BWG/feed arrangement, thermal gradients, quasi-static wind effects and atmospheric refraction. In fact, the servo system applies an offset to the commanded azimuth and elevation positions according to the measured or derived pointing error values. Tiltmeters mounted at the elevation axis and linked to the

servo system, measure the quasi-static tilt of the antenna tower and the azimuth housing due to thermal effects and wind.

Thermal effects impacting the elevation part are compensated in real-time: the deformation of the main- und subreflector supporting structure is predicted by evaluating a Thermal Distortion model of the elevation part, which uses as input the readout of 252 temperature sensors mounted to the main- and subreflector supporting structure.

Table 2: Approximate magnitude of the uncompensated raw systematic pointing errors.

Pointing Error Source	Approximate Magnitude [mdeg]	Estimation Method
Refraction	85 at 10 deg elevation 300 at 2 deg elevation	Modelled, measured
Gravity	80	Measured
Misalignments, RF beamsquint	15 (total)	Measured
Thermal deformations of azimuth housing	6	Measured
Thermal deformations of main reflector	2	Modelled, measured
Quasi-constant wind	2	Modelled
Wind Gusts (mechanical and servo)	3	Modelled

Systematic pointing errors like gravity effects, mechanical misalignments, etc. are compensated by a Systematic Pointing Error Model (SPEM). This model consists of a set of linear-independent mathematical terms, which describe the impact on the pointing of the gravity effect, misalignment, frequency band and polarization dependent RF beam squint, etc as function of the azimuth and elevation angle [4]. The coefficients, which determine the weight of each term respectively each effect, are determined by evaluating pointing measurements using radio stars.

For DSA1, a prototype Pointing Calibration System (PCS), which automates the scanning of radio star measurements, was developed and tested. For DSA2, an operational PCS was developed and integrated with the servo system [3]. This system is used to perform pointing error (PE) measurements, calculate SPEM coefficients from the PE measurements and forward the new coefficients to the Antenna Control Unit. The DSA2 PCS fully automates pointing error measurements and provides an easy tool for the calculation of the SPEM coefficients. This is considered as prerequisite to have the optimum pointing performance also during day-to-day operations.

The antenna system employs an automatic subreflector positioner system, which corrects the position of the subreflector to compensate the deflection of the main reflector and the subreflector lag over the elevation travel range. This is particularly important for Ka-band. Over the 90° elevation range, the position of the passive subreflector can vary by up to 12 mm. This deflection also causes the subreflector to tilt. The effect on antenna performance is to alter the pointing direction (which the antenna servo system can compensate for), and more importantly, to degrade the antenna efficiency. At X-band, the gain can be reduced by up to 0.7 dB from the value at which the subreflector is aligned. For Ka-band operation, the efficiency degradation, if not compensated, would result in a gain loss of more than 5 dB. The implemented subreflector positioning system automatically repositions the subreflector to within 0.05 mm of its optimum position as the antenna elevation changes.

The third 35m deep space antenna is planned to be erected in Chile and therefore is exposed to very high seismicity. For this reason intensive seismic analyses with response spectrum technique are going to be performed within a seismic load study. The actual software and hardware equipment allows the computation of much larger Finite Element models compared to those of the DSA1 and DSA2. For that reason the mesh of the existing Finite Element models of the DSA2 were refined and the extended actual models of the DSA3 consist of approx. 130 000 elements with approx. 123 000 nodes and approx. 700 000 local degrees of freedom.

SYSTEM PERFORMANCE

In Fig. 5, the predicted surface accuracy versus elevation of the main reflector is shown. The surface accuracy of the main-reflector panels, which have a surface accuracy r.m.s. due to fabrication of 0.08 mm (measured) deteriorates due to the wind and thermal loads to approximately 0.2 mm. (predicted by Finite-Element Analysis). The main reflector supporting structure deformation contributes with less than 0.2 mm to the total surface accuracy. The predicted total surface accuracy r.m.s is always better than 0.3 mm even for worst case wind and thermal conditions and better than 0.2 mm for benign conditions. Surface accuracy measurements performed with photogrammetry at 0 and at the rigging angle of 41 deg elevation confirm the predicted results. An r.m.s. surface accuracy error of 0.165 mm at 0 deg elevation has been measured for night time conditions without wind (Fig. 6). At the rigging position, the measured r.m.s. surface accuracy of 0.089 mm is limited by the measurement accuracy of the photogrammetry approach. In [6], the surface accuracy of the main reflector of the 34 m JPL DSN DSS-24 antenna has been measured with holography technique. At 12.5 deg elevation, the r.m.s. surface accuracy due to gravity deformations is 0.26 mm, which is nearly twice as much as the surface error of the ESA deep space antennas.

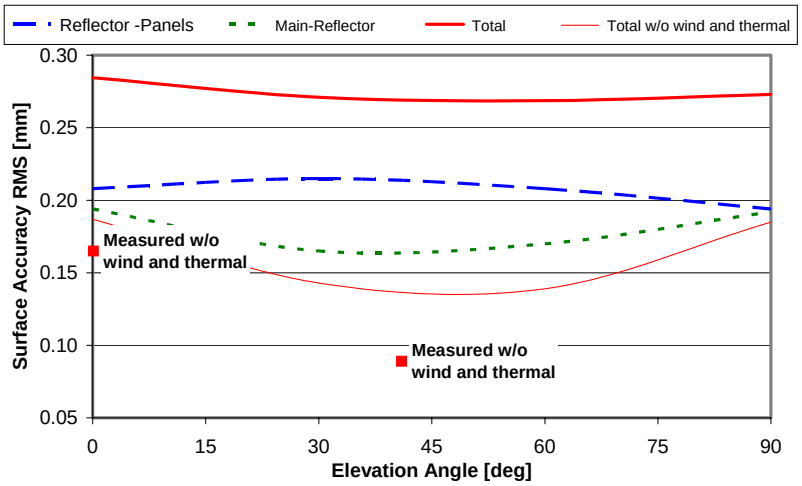

Figure 5: Main reflector surface error versus elevation angle. The contribution of the reflector panels and the main reflector backup structure is shown for the worst case load case including gravity, wind and thermal effects. Additionally, the measured surface accuracy for 0 and 41 deg elevation is shown (backup structure only).

For the subreflector, a shaped hyperboloid with 4.2 m diameter, the fabrication errors dominate the achievable surface accuracy. It is therefore constructed of cast and welded aluminium (DSA1) and welded aluminium only (DSA2). This construction method allows the very tight surface accuracy requirements to be met. A subreflector r.m.s. surface accuracy error of 0.065 mm at 41 deg elevation is achieved for night time conditions without wind.

Pointing measurement using the PCS of DSA2 shows that the residual pointing error in both X and Ka-band is less than 4 mdeg (99 % probability of occurrence, 10 deg elevation to 90 deg elevation) under benign conditions. Fig. 7 shows a set of Ka-band pointing error measurement results from February 2006. The measurement conditions were optimal: cold and cloudless sky. Based on these measurements, which were running 12 hours, the Mean Radial Error (MRE) is 1.32 mdeg. To demonstrate the achievement: the MRE values reported in [7] for the 34m BWG antennas of the DSN based on comparable measurements vary from 4.34 mdeg to 7.50 mdeg. Simulations have shown that the overall pointing accuracy degrades by approximately 2 mdeg under worst-case wind and thermal conditions. Recent observations, where the wind direction with respect to the elevation and azimuth position of the antenna presented the worst case, confirm the predictions. The servo position errors for wind speeds below 60 km/h are below 4 mdeg (Fig. 8) leading to an overall pointing accuracy better than 6 mdeg with a probability of occurrence of 99 % under worst case environmental conditions (MRE ≈ 2.5 mdeg).

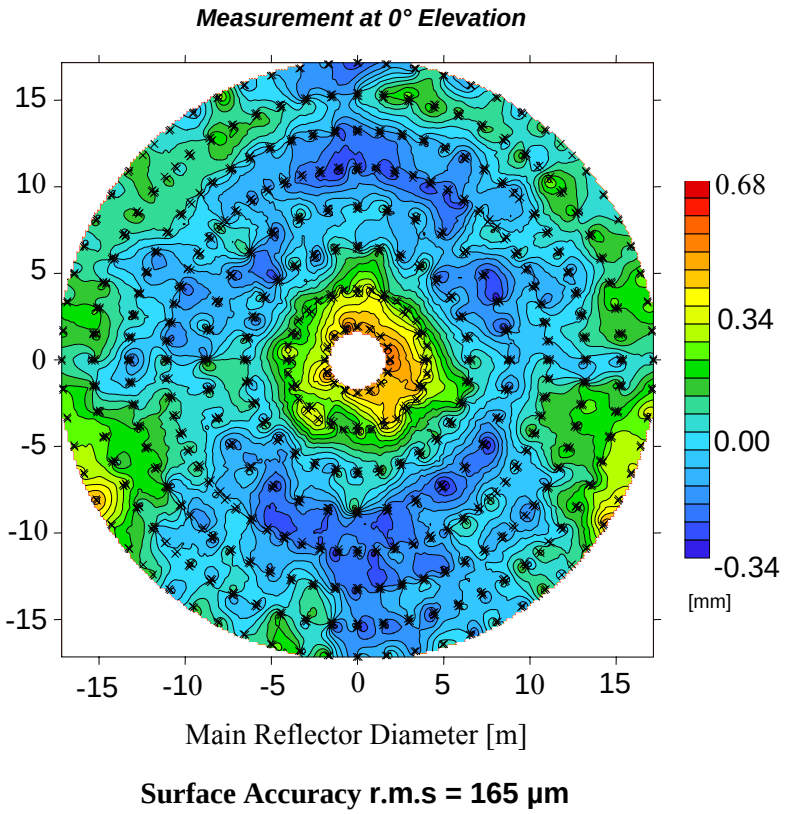

Figure 6: Contour plot of the surface accuracy measurements performed with photogrammetry at 0 deg elevation.

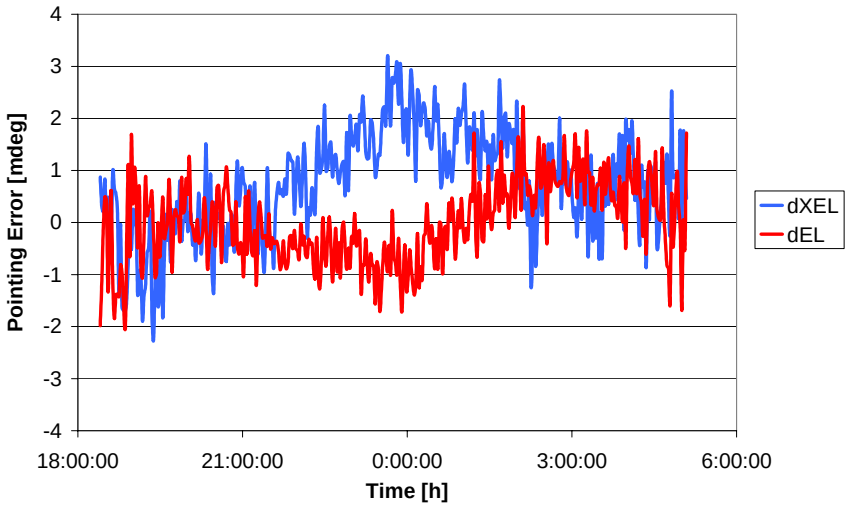

Figure 7: Measured pointing error in elevation axis (dEL) and cross-elevation axis (dXEL) after applying all pointing error compensation methods when tracking a radio star for a period of 12 hours.

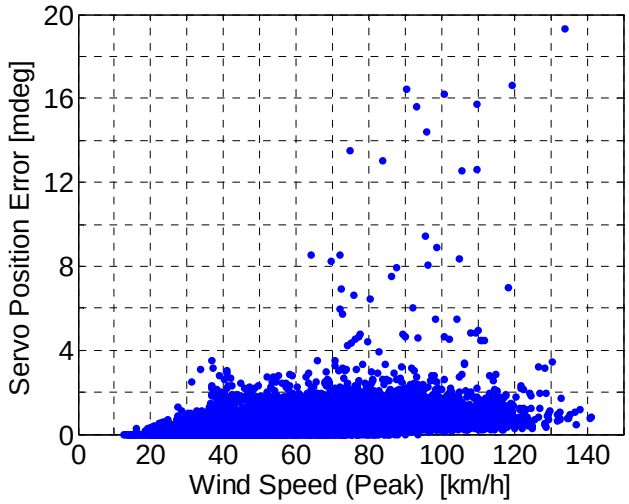

Figure 8: Servo position error versus wind speed (peak). The wind direction with respect to the elevation and azimuth position of the antenna presented the worst case. The position errors have been taken directly from the position control loop. The wind speed has been measured with an ultrasonic wind sensor with a sampling rate of 10 samples/sec.

CONCLUSION

The surface accuracy and pointing accuracy requirements applicable to ESA's 35 m deep space antennas demanded for a state-of-the-art design approach. By means of an extensive use of simulation tools, the antenna structure has been optimized to achieve the specified surface accuracy of 0.3 mm r.m.s and the pointing accuracy of 5.5 mdeg under worst case conditions with a cost effective light-weight steel structure. Photogrammetry measurements of the main- and sub-reflector surface and pointing error measurements using the Pointing Calibration System (PCS) confirmed the predicted results. Measurements of the servo performance during a period with worst case wind have been used to verify the magnitude of the anticipated servo position errors.

REFERENCES

[1] M. Warhaut, R. Martin, "Europe accesses to deep space at New Norcia (Western Australia)", ESA Bulletin 114, 2003.

[2] D. A. Akins, R. Martin, "ESA 35m deep space antenna front end system", Eight International Conference in Space Operations, Space Ops 2004 Montreal.

[3] R. Osterried, P. Droll, R. A. Plemel, "ESA DSA2 Pointing Calibration System", Progress Reports – Selected papers from SpaceOps 2006, to be published.

[4] P. Stumpff, "Astronomical Pointing Theory for Radio Telescopes", Klein-Heibacher Berichte, Vol. 15, Fernmeldetechnisches Zentralamt, Darmstadt, Germany, pp. 431-437, 1972.

[5] W. Gawronski, "Control and Pointing Challenges of Antennas and (Radio) Telescopes", IPN Progress Report 42-159, 2004.

[6] D. J. Rochblatt et al. "DSS-24 Microwave Holography Measurements", TDA Progress Report 42-121, 1995.

[7] DSMS Telecommunication Link Design Handbook, "302 – Antenna Positioning", 810-005, Rev. E, 2004.